ION SOURCES

N. Angert
GSI, Darmstadt, Fed. Rep. Germany

1. INTRODUCTION

Ion sources are used in many research fields such as mass separation, ion implantation, fusion, atomic physics, and a variety of accelerators for nuclear and particle physics with different requirements. The large proton accelerator facilities need beams of hundreds of milliampere protons, and recently H^- beams have become attractive. Tandem accelerators also start with negative ions of hydrogen, and with heavy ions which are then stripped to high charge states. During the last decade there was an increasing interest in medium- and high-energy heavy-ion beams. The design of injector accelerators for this application is strongly influenced by the charge states which can be achieved in the heavy-ion sources.

This paper cannot deal with all the different types of ion sources used for accelerators, but it will try to give an idea of the different types involved and will explain the principles of the most important ones.

2. PRINCIPLES

2.1 Production of positive ions

Positive ions can be created by supplying the ionization energy by means of photons and electrons or by contact ionization on surfaces. For the sources discussed here, bombarding electrons are used. The basic process is

$$e + A \rightarrow A^{+} + 2e \ , \tag{1}$$

or for multicharged ions

$$e + A^{i+} \rightarrow A^{(i+1)+} + 2e \ , \tag{2}$$

assuming only outer-shell step-by-step ionization and neglecting, for example, Auger processes etc.

Figure 1 shows the ionization energies against nuclear charge for different ionization states, whilst in Fig. 2 the ionization cross-section versus bombarding electron energy is shown for different charge states of argon. From the latter it can be seen that, after a steep increase, the cross-section for a certain charge state reaches its maximum at about three times the ionization potential; it decreases with increasing charge state and, slowly, with increasing energy of the bombarding electron. For high production of a charge state, the electron energy should be about three times the ionization potential. This means 10 to 40 eV for singly charged ions, several hundred eV for multicharged states, and keV to tens of keV for highly charged ions.

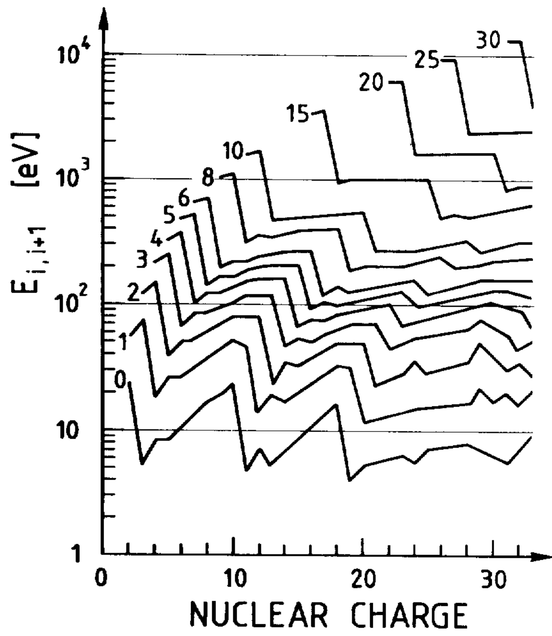

Fig. 1 Ionization energies for step-by-step ionization of elements up to nuclear charge 30

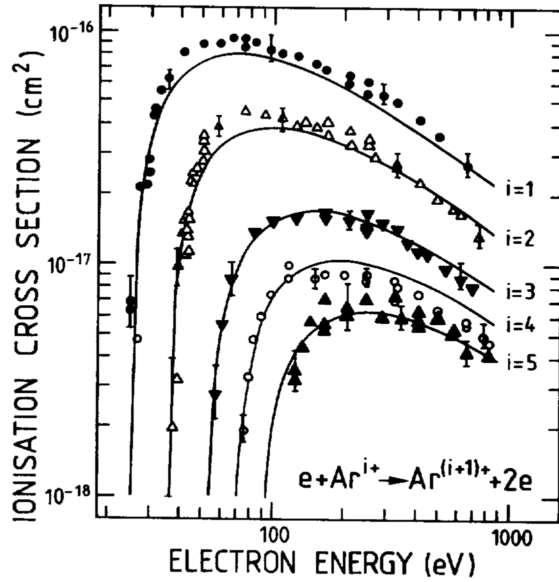

Fig. 2 Ionization cross-section versus bombarding electron energy for different charge states of argon

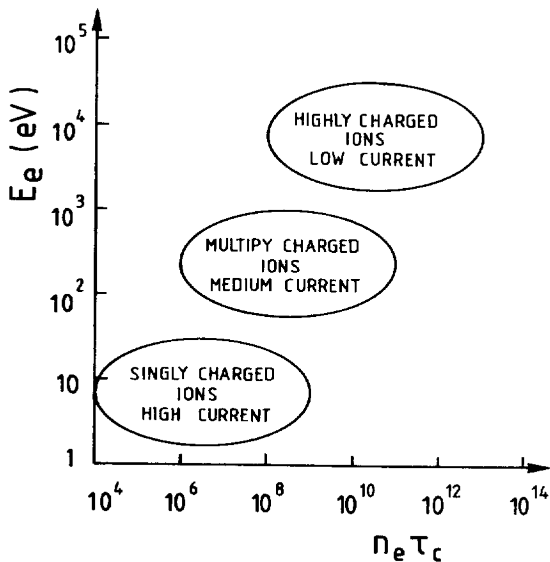

Fig. 3 Operating parameters for different types of ion sources. Electron energy versus electron density times containment time

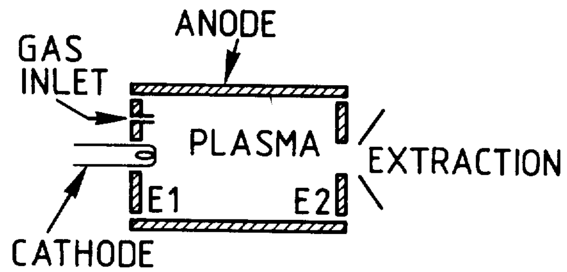

Fig. 4 Schematic of a high-current source. End-plates E1 and E2 can be part of the anode, floating, or near cathode potential

The time necessary for an atom to reach a certain charge state depends on the cross-section and the electron current density. However, ion-loss processes are in competition with the ionization. Ions are lost by diffusion out of the ionization volume or by charge-exchange processes with neutral atoms. Taking this into account, the time evolution of the charge-state distribution can be calculated from the following simplified differential equation[1]):

$$dn_0/dt = n_0\sigma_{0,i}j_e \tag{3a}$$

$$dn_i/dt = n_{i-1}\sigma_{i-1,i}j_e - n_i\sigma_{i,i+1}j_e - n_i/\tau_c(i) \ , \tag{3b}$$

where

n_0 is the neutral particle density,

n_i is the ion density in charge state i,

$\sigma_{i-1,i}$ is the cross-section for single-step ionization into charge state i,

j_e is the electron current density,

$\tau_c(i)$ is the lifetime of ion in charge state i.

The charge-state distribution is mainly determined by σ, i.e. by the energy of the electrons, and by $j_e\tau_c$, the product of electron current density and containment time. The diffusion time out of the ionization volume without any confinement is in the range of microseconds but, by using special magnetic and electric fields, containment times of up to seconds can be achieved. The dominant charge-exchange process is with neutral atoms, that between ions being much smaller because of Coulomb repulsion. The lifetime is in the range of milliseconds for residual gas pressures below 10^{-6} - 10^{-7} Torr[2]). From Eq. (3) one can draw the following conclusions:

i) high j_e and n_0 lead to high current, but not to high charge states because of short τ_c;
ii) high electron energy, low pressure, and long containment are needed for high charge states.

This leads to the schematic diagram shown in Fig. 3, where $n_e\tau_c = j_e\tau_c/v_e$ (v_e electron velocity) is taken for the abscissa and $n_e\tau_c$ is a figure of merit as used in fusion reactors.

2.2 Production of negative ions

The process involved in the attachment of an electron to a neutral atom is exothermic, in contrast to the endothermic processes required for positive ion formation. The electron affinity, defined as the difference between the ground-state neutral E_0 and the negative ion E_n energies

$$E_A = E_0 - E_n \ , \tag{4}$$

is a measure of the stability and ease of ion formation. Table 1 displays atomic electron affinities[3]), the positive values indicating ion stability and vice versa. In addition to

the formation of negative atomic species, many negative molecular ions have been observed. There is also an important class of negative ions which are only formed in excited metastable states.

Table 1

Electron affinities and ionization energies of elements

(Each cell: atomic number and symbol, ionization potential, electron affinity)

GROUP I A	II A	III A	IV A	V A	VI A	VII A	VIII A
1 H 13.595 0.7542							2 He 24.58 0.078*
3 Li 5.39 0.620	4 Be 9.32 < 0	5 B 8.30 0.28	6 C 11.26 1.268	7 N 14.54 < 0	8 O 13.61 1.462	9 F 17.42 3.399	10 Ne 21.56 < 0
11 Na 5.14 0.548	12 Mg 7.64 < 0	13 Al 5.98 0.46	14 Si 8.15 1.385	15 P 10.55 0.743	16 S 10.36 2.0772	17 Cl 13.01 3.615	18 Ar 15.76 < 0
19 K 4.34 0.5012	20 Ca 6.11 < 0	31 Ga 6.00 0.3	32 Ge 7.88 1.2	33 As 9.81 0.80	34 Se 9.75 2.0206	35 Br 11.84 3.364	36 Kr 14.00 < 0
37 Rb 4.18 0.4860	38 Sr 5.69 < 0	49 In 5.78 0.3	50 Sn 7.34 1.25	51 Sb 8.64 1.05	52 Te 9.01 1.9708	53 I 10.45 3.061	54 Xe 12.13 < 0
55 Cs 3.89 0.4715	56 Ba 5.21 < 0	81 Tl 6.11 0.3	82 Pb 7.41 1.1	83 Bi 7.29 1.1	84 Po 8.43 1.9	85 At 9.5 2.8	86 Rn 10.74 < 0

III B	IV B	V B	VI B	VII B	VIII B			I B	II B
21 Sc 6.56 < 0	22 Ti 6.83 0.2	23 V 6.74 0.5	24 Cr 6.76 0.66	25 Mn 7.43 < 0	26 Fe 7.90 0.25	27 Co 7.86 0.7	28 Ni 7.63 1.15	29 Cu 7.72 1.226	30 Zn 9.39 < 0
39 Y 6.5 = 0	40 Zr 6.95 0.5	41 Nb 6.77 1.0	42 Mo 7.18 1.0	43 Tc 7.28 0.7	44 Ru 7.36 1.1	45 Rh 7.46 1.2	46 Pd 8.33 0.6	47 Ag 7.57 1.303	48 Cd 8.99 < 0
57 La 5.61 0.5	72 Hf 7. < 0	73 Ta 7.88 0.6	74 W 7.98 0.6	75 Re 7.87 0.15	76 Os 8.7 1.1	77 Ir 9. 1.6	78 Pt 8.96 2.128	79 Au 9.22 2.3086	80 Hg 10.43 < 0

*METASTABLE

Negative ions may be formed by means of several physical or physico-chemical mechanisms such as volume processes by electron impact and charge exchange in metal vapours and on surfaces. Compared with positive ion production there is a large variety of processes, but only a few will be considered here.

2.2.1 *Volume processes*[4)]

Dissociative Attachment: Electrons are stably attached to atoms during their interactions with molecular neutrals according to the following reaction:

$$e + XY \rightarrow X^- + Y \,, \tag{5a}$$

or

$$e + X_2 \rightarrow X^- + X \,. \tag{5b}$$

Polar Dissociative Attachment: In this case the electron is not captured but excites only the molecule to an unstable state,

$$e + XY \rightarrow X^+ + Y^- + e \,. \tag{6}$$

Ternary Collision: This is most efficient in dense gas at low electron energies and is described by the reaction:

$$e + X + Y \rightarrow X^{-} + Y \ . \qquad (7)$$

2.2.2 *Charge-exchange processes in metal vapour*[5]

Charge-exchange processes in alkali or alkaline-earth vapour targets result in a fraction of a positive ion beam being converted into negative ions with a conversion efficiency ranging from 0.5 to > 90%[6,7]. This mechanism offers a practical and efficient means of producing useful beams from elements which have negative electron affinity.

2.2.3 *Processes on surfaces*[8]

Interaction between sufficiently energetic particles and a surface having a low work function can result in the formation of negative ions. This effect can be enhanced by alkali coating the surfaces exposed to the bombardments. There are two principle processes, namely:

i) the thermodynamic equilibrium surface ionization, where the slow atom or molecule impinging on the surface is emitted as a positive or negative ion after a mean residence time;

ii) the non-thermodynamic atom-surface interaction, where negative ions are produced by sputtering a material in the presence of an alkali metal[9].

3. ION SOURCES FOR POSITIVE IONS

3.1 High-current sources

In its simplest form a high-current ion source consists of a cathode filament surrounded by an anode cylinder or cube and a single or multiple aperture extraction plate opposite the cathode (Fig. 4). The end-plates E1 and E2 can be at anode, floating, or near-cathode potential in order to reflect the electrons that are needed to provide a higher ionization efficiency. Discharge is ignited at a gas pressure of 10^{-1} to 10^{-2} Torr, and a high discharge current is necessary because of the large anode area. With the availability of strong permanent magnets, multicusp sources are becoming popular for creating the plasma needed for high-current sources of singly charged ions. The discharge vessel is surrounded by magnets with alternating polarity, creating a minimum-B configuration which reduces the effective anode area and yields a quiet, homogeneous plasma of large cross-sectional area. Figure 5 shows a cubic multicusp source[10]. A cylindrical version[11] of the reflex type is shown in Fig. 6 together with its multipole field configuration. This source was especially developed for singly charged, high-current, heavy-ion beams of up to 100 mA operating with discharge voltages and currents of 10-100 V and 20-150 A, respectively. Details of further high-current sources can be found elsewhere[11].

3.2 Duoplasmatron

An ion source which has been in use for many years, both for the production of high-current proton beams and for lowly charged positive heavy ions, is the duoplasmatron source[12] shown in Fig. 7. The discharge plasma is sustained by a thermionic cathode and is radially

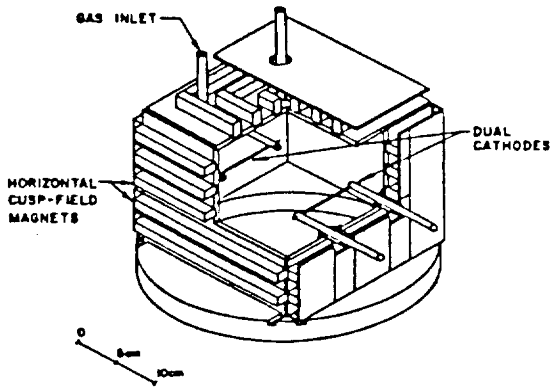

Fig. 5 Multicusp ion source. Ions are extracted towards the bottom

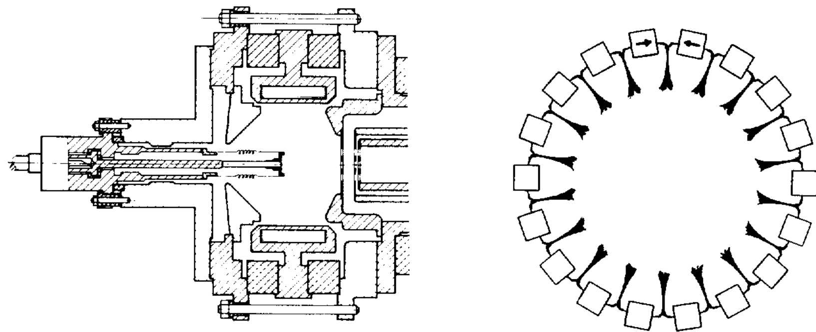

Fig. 6 Multicusp ion source for heavy ions

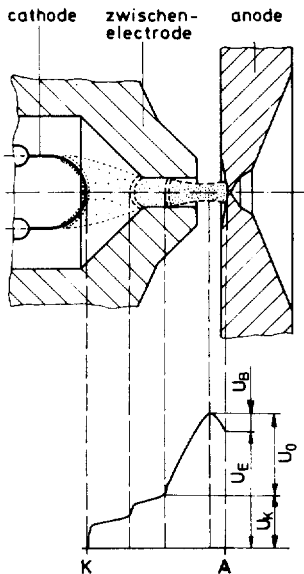

Fig. 7
Discharge region of duoplasmatron and potential along discharge

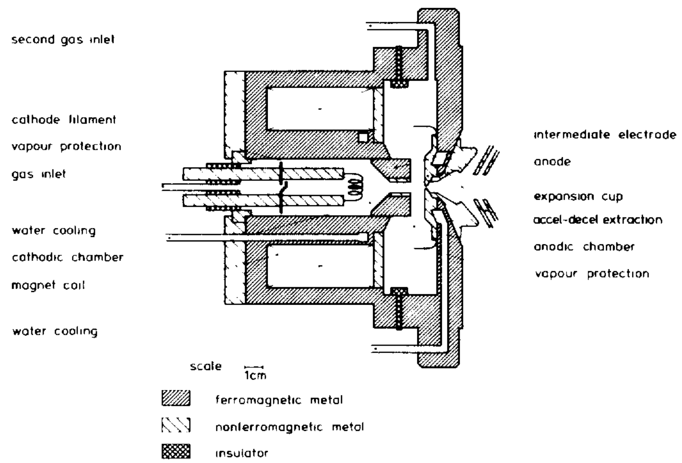

Fig. 8 GSI duoplasmatron for multicharged ions

compressed by means of an intermediate electrode and an axial magnetic field. The anode and the intermediate electrode are made from ferromagnetic material and form the pole pieces of a magnetic yoke. Owing to the constrictions of the discharge, one or more double layers are generated along the plasma column, separating regions of different neutral pressure and plasma density. Near the anode there exists a relatively dense plasma with a high degree of ionization, whose potential is higher than that applied to the anode[13]. The ions are extracted through a small outlet aperture in the anode. Figure 8 shows a design developed at GSI for multiply charged ions[14], which has a specially shaped magnetic field whose maximum value is near the anode orifice. The intermediate electrode channel is only 5 mm in diameter in order to achieve a higher plasma column impedance and thus higher discharge voltages and electron energy, these in turn creating higher charge states. Typical discharge voltages and currents are in the range up to 250 V and 20 A, respectively. This results in electron current densities j of more than 100 A/cm^2. The residual gas pressure is estimated to be about 10^{-2} - 10^{-3} Torr. However, the containment time is only microseconds and, for example using xenon and milliampere intensities, the maximum charge states obtained are not more than 10+. Special designs for protons deliver several hundred mA of beam.

3.3 PIG (Penning Ion Gauge) source

Figure 9 shows the principle of a PIG source for multicharged ions. It consists of the two cathode blocks and a cylindrical anode in a magnetic field parallel to the anode axis. A discharge is ignited by increasing the gas pressure in the anode cylinder and raising the voltage between the cathode and anode. Contrary to the duoplasmatron source, where the electrons pass only once from the cathode to the anode, in the PIG source they are emitted from one cathode, follow the B-field lines to the other cathode, and are then reflected there. They oscillate in this way a few times through the discharge, thereby increasing the electron current density. Ions can be extracted either axially, through a hole in one cathode or, more commonly, radially through a slit in the anode, using the magnetic field simultaneously for charge analysis.

To obtain the maximum value for the total ionization cross-section, and hence the maximum production rate for the ions, the electrons must have about three to five times the ionization energy for step-by-step ionization of the charge state considered. Therefore, it is advantageous to control the arc impedance and hence the electron energy. This can be done by additional heating of one cathode by an electron current from a filament. The output is then optimized by proper choice of arc-current, cathode heating, and gas flow, which corresponds to neutral density. These parameters influence the electron density, electron energy, and charge-exchange losses. Figure 10 shows the PIG source used at the Unilac. The top cathode is heated by electron bombardment, whereas the so-called anticathode is cooled. Solid materials can be fed into the discharge by sputtering from an electrode negatively biased with respect to the anode. This type of source has been adopted from Orsay[15] and is based on the Dubna design[16,17]. The output of the PIG source is about 100 times higher than from a duoplasmatron for charge states 7+ to 10+. Typical discharge voltages and currents are in the range up to 2000 V and 10 A, respectively. The residual gas pressure is estimated to be about 10^{-4} to 10^{-3} Torr.

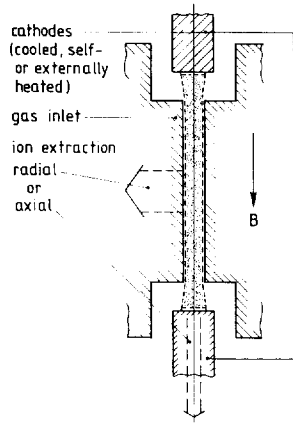

Fig. 9 Schematic of PIG sources

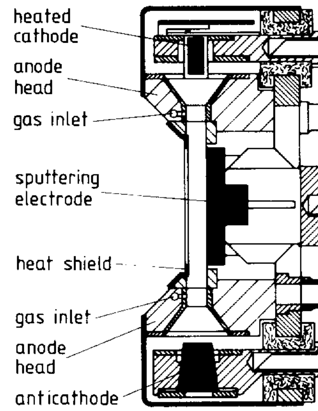

Fig. 10 GSI PIG source

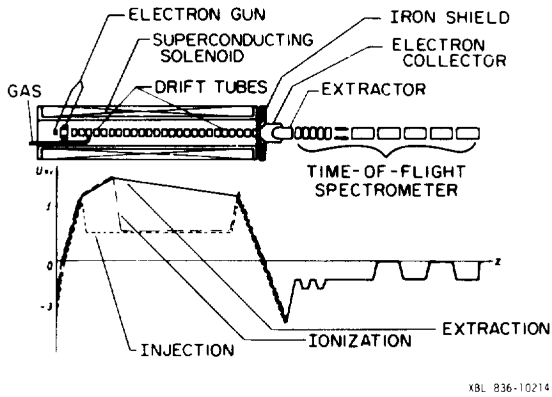

Fig. 11 Schematic drawing of Krion EBIS source and potential distribution for different operating steps

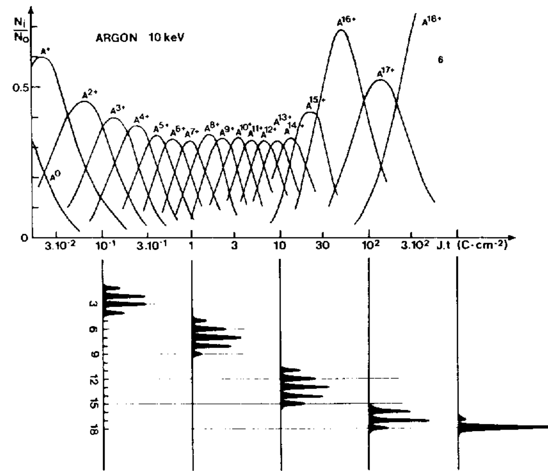

Fig. 12 Development of charge-state distribution of argon with the production jτ with a 10 keV electron beam

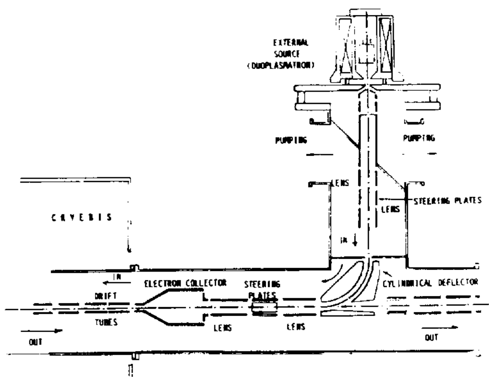

Fig. 13 Saclay external ion injection into EBIS source

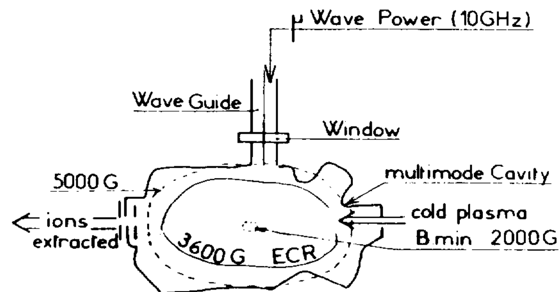

Fig. 14 Schematic of the ECR ion source

3.4 Electron beam ion source (EBIS)

In the plasma sources discussed above, the ionizing electrons gain their energy in plasma sheaths, and the value of the energy depends on the plasma parameters. In an EBIS (Fig. 11) an external electron gun launches a small-diameter electron beam into the ionization volume down the axis of a solenoid[18]. The beam stops on the electron collector in the magnetic stray field. The potential along the axis is defined by a number of cylindrical drift tubes. The ions are contained radially in the electrostatic potential well of the electron beam and axially by the potential barriers on the end drift tubes. During a short 'injection' period, the desired number of ions is accumulated in the well. Then the potential distribution is switched to the 'ionization' mode, in which the first barrier is moved downstream to prevent additional low charge-state ions from entering the containment volume. When the average charge state has reached the desired value, the potentials are switched to the 'extraction' mode. This applies a potential ramp accelerating the ions into the extractor. Typical extraction times are about 50 μs, at 1-10^3 Hz repetition rate.

The EBIS is an almost ideal source for very high charge states. Commonly operated at very low residual gas pressures down to 10^{-10} Torr, and based on very good radial and axial confinement, containment times up to seconds can be achieved. In addition, high electron energies can be applied. Figure 12 shows a calculated evolution of charge-state population with the product $j_e\tau_c$ for Ar with a 10 keV electron beam[19]. For source parameters of 10 keV, 1 A electron beam, and 1 m length, the theoretical number of ions is $10^{11}/i$, where i is the average charge state. Actual sources achieve about 10% of the theoretical values[20]. In addition to the 'injection' mode described above, ion injection from an external source (Fig. 13), which allows also the use of solid material elements, has been successfully tested[21]. Most EBIS sources have superconducting solenoids[18,20,22,23].

3.5 Electron cyclotron resonance (ECR) ion source

In an ECR source the ionizing electrons do not gain the desired energies in a plasma sheath or by electrostatic acceleration from a cathode; instead, the electrons of the plasma itself are accelerated by an oscillating electromagnetic wave[19]. If a metallic box (see Fig. 14) is filled with microwave power (e.g. f = 10 GHz, λ = 3 cm) and is large with respect to λ, it can be considered as a multimode cavity. If this box is put into a minimum-B structure where the magnetic field strength is between 0.2 and 0.5 T, there must be a magnetic surface where the field strength is B_0 = 0.36 T and the gyrofrequency of the electrons 10 GHz. Such a surface creates an electron cyclotron resonance, as there is always a component of the electric field perpendicular to the magnetic field in a multimode cavity. If the electrons pass many times through this surface, they are stochastically heated.

Figure 15 shows the two-stage MICROMAFIOS source of Geller[19]. A plasma is produced in the first stage at high pressure (10^{-2} - 10^{-3} Torr) by microwave power in an axial magnetic field from which the cold plasma diffuses into the second stage. Here the ionization to high charge states is done by the energetic electrons of up to several tens of keV created by the ECR process. The background pressure in this stage must be < 10^{-6} Torr to prevent charge-exchange losses. For a long confinement time of the ions against plasma instabilities, a sextupole field is superimposed on the basic mirror configuration of the second stage, in a minimum-B configuration.

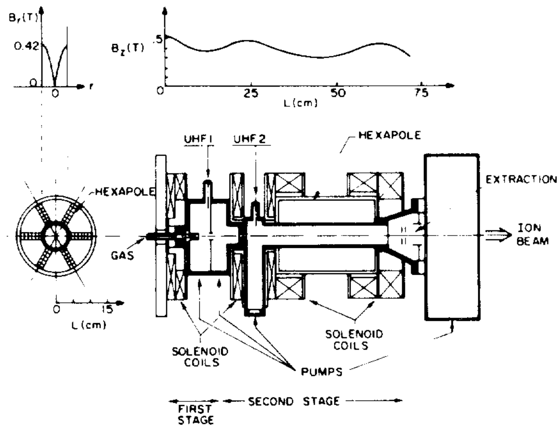

Fig. 15 The two-stage MICROMAFIOS ECR source of Geller

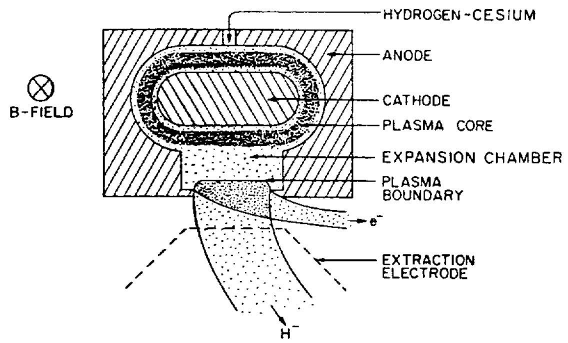

Fig. 16 Schematic drawing of a magnetron source

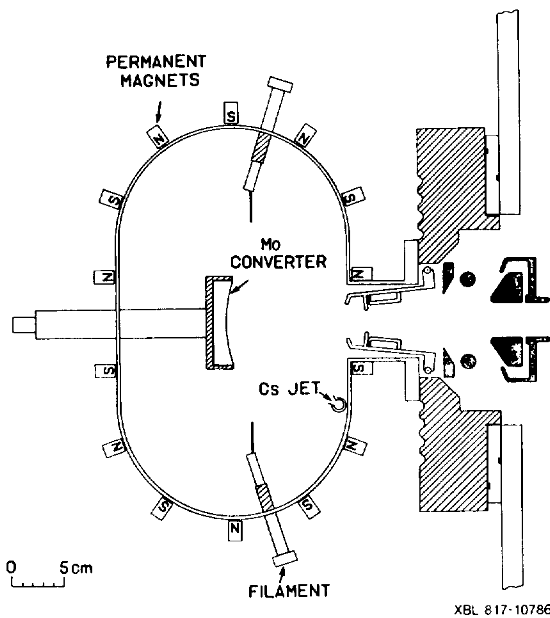

Fig. 17 LBL multicusp source for H^- ions

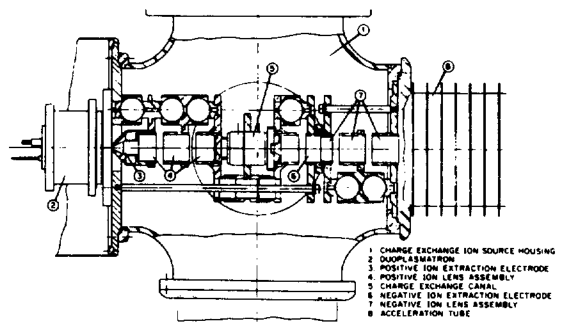

Fig. 18 Schematic drawing of a duoplasmatron charge-exchange source at Oak Ridge

The ECR source can be operated both in CW and pulsed mode. The latter offers 3-5 times enhanced yield for high charge states of light ions. For instance, 100 μA O^{6+} could be achieved in this mode. The CW mode makes it an attractive source for upgrading cyclotrons for heavy ion operation. A superconducting ECR source has also been built in Louvaine-la-Neuve and is used in a cyclotron injector system[24].

4. ION SOURCES FOR NEGATIVE IONS

4.1 Magnetron source

Today, H^- ions are very important both for injection into circular accelerators, where by stripping to H^+ the injection is not limited by Liouville's theorem, and for H^0 injection in fusion devices. About 10 years ago, most H^- sources were adapted positive-ion devices (duoplasmatrons, Penning sources) [25]. This has changed with the discovery that in a magnetron source H^- can be very efficiently produced on low-work-function, caesiated surfaces[26] (a method now also adopted by Penning[27] and multicusp[28] sources).

Figure 16 shows a schematic of a magnetron source. In a magnetic field of 1-2 kG a discharge is established between a cold cathode and anode mounted in such a way that there exist closed E × B loops around the cathode. Electrons emitted from the cathode by secondary and photoelectric emission are accelerated by the cathode fall and bent by the magnetic field, describing cylindrical trajectories around the cathode. Caesium is fed into the discharge and is deposited on the cathode, creating the required conditions for surface production of H^- ions. Most existing magnetron sources incorporate two substantial improvements:

i) the cathode surface opposite the extraction slit has the shape of a cylindrical groove so that the produced H^- ions are focused into the extraction slit;
ii) the gap between the cathode and the anode is not uniform[29].

In this way current densities up to 3 A/cm^2 can be achieved.

4.2 Multicusp source with a converter

The multicusp source shown in Fig. 17 has been developed for fusion applications[28], but may also be used for accelerators. The permanent magnets create the multipole field which is necessary to create a uniform and stable plasma. The discharge is maintained by several hot filaments. A molybdenum converter is mounted near to the centre of the source, with a curvature such that negative ions produced at its surface are focused into the extraction slit. The source is operated at a hydrogen pressure of about 10^{-3} Torr, with caesium vapour introduced into the discharge.

4.3 Charge-exchange sources

Sources of this type consist of a positive ion source (for instance, duoplasmatron) and a charge-exchange canal where the exchange interactions take place. The exchange canal is usually a tube, ∿ 0.75 cm in diameter and ∿ 5 cm in length, to which is attached a gas line or an oven for introducing the gaseous or solid exchange material. The canal region can be biased negatively with respect to the source at ground potential, or at ground potential with a positively biased source. The former configuration permits the extraction of

negative ions which are created by the positive ion beam from the exchange material itself[30]. Figure 18 shows a schematic drawing of the Oak Ridge type source[3]. In this particular mode of operation the formation processes are not through charge exchange but polar dissociation, dissociative attachment, and ternary collisions (the reactions described in subsection 2.2.1). In the exchange mode (exchange canal at ground potential), the use of universal-type positive ion sources permits the generation of negative ions from any element which has a positive electron affinity [Eq. (4)], and also of metastable negative ions.

4.4 Surface ionization sputter sources

Several versions of negative ion sources are based on the fact that the negative ion yield of sputtered particles is greatly enhanced by the presence of a thin layer of caesium on the surface of the material being sputtered[31]. A schematic of one of the most versatile negative-ion sputter sources is shown in Fig. 19. It uses a caesium surface ionization source at ground potential. A caesium beam of 0.1 to 1 mA is accelerated to $\sim$ 20 keV and strikes a conical surface of $\sim$ 20° half angle. The caesium serves both for sputtering and as an electron donor in the formation of negative ions, the latter being extracted through an aperture in the end of the cone. The source is equipped with an external indexed wheel which permits rapid change of ion samples. With this source, currents in the range from 1 to 100 μA can be achieved, depending on the species.

5. BEAM FORMATION

Most of the ion sources considered so far are plasma sources from which the ions are extracted through circular or slit apertures by applying a voltage. The principles of the ion optics involved are derived from those of electron guns. New investigations have been stimulated during the past 10 years by the development of high-intensity beams for fusion application. Here only a few principles will be reviewed, further information being available elsewhere[32,33].

In a simple idealized model[32] (Fig. 20) the ions are emitted from a curved plasma boundary established by the balance between plasma pressure and the applied voltage. As a result, the ions converge toward this electrode before diverging as they pass through the aperture in the second electrode, this aperture being an electrostatic lens. The saturated ion current density J_s which can be extracted from a plasma boundary is

$$J_s = n_i \, e(kT_e/M)^{1/2} . \tag{8}$$

Thus the total current is $I = \pi r_1^2 J_s$.

The current I (A) is related to the applied voltage U (V) by the equation

$$\frac{I}{U^{3/2}} \left(\frac{M}{i}\right)^{1/2} = P_0 \left(\frac{A}{V^{3/2}}\right) = 1.72 \times 10^{-7} \left(\frac{r_1}{d}\right)^2 , \tag{9}$$

where P_0 is the perveance for plane parallel electrodes, whilst M and i are the ion mass and charge, respectively.

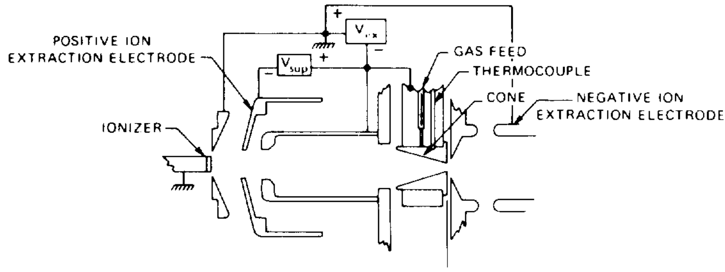

Fig. 19 Schematic drawing of the Middleton-Adams sputter source for negative ions

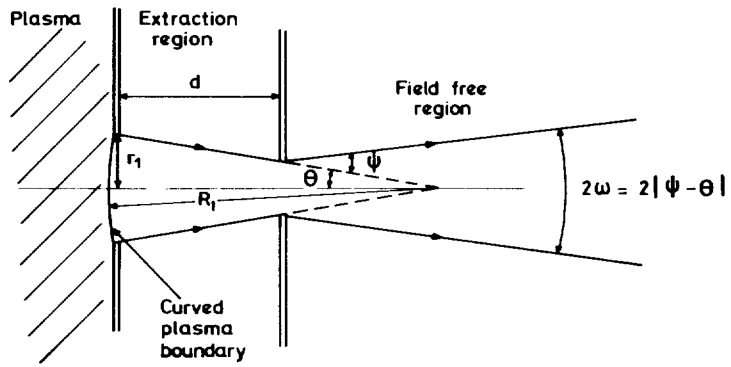

Fig. 20 Scheme of ion optics in beam extraction region

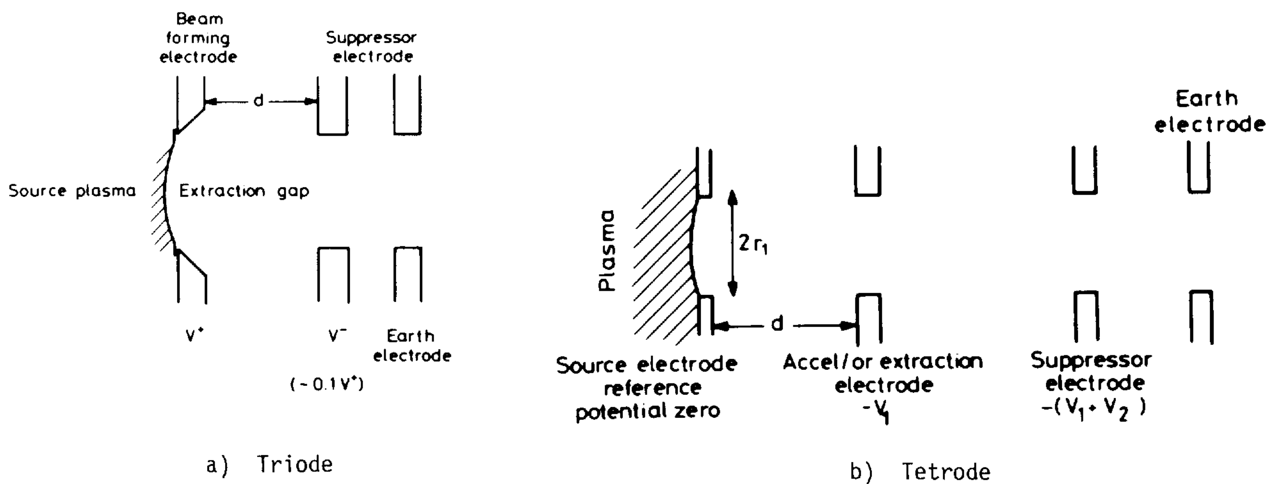

a) Triode

b) Tetrode

Fig. 21 Schematic drawings of commonly used acceleration electrode systems

For a curved plasma boundary we can consider the current flow from a small circular area of a spherical surface. This results in a perveance of

$$P_S = P_0(1 - 1.6\ S\theta)\ , \tag{10}$$

where the aspect ratio $S = r_1/d$, and θ as defined in Fig. 20 is the convergence angle toward the extraction electrode. Taking into account the lens effect of the extractor, the resulting beam divergence ω is given by

$$\omega = 0.29\ S(1 - 2.14\ P/P_0)\ \text{rad}\ . \tag{11}$$

This equation predicts that $\omega = 0$ for $P = 0.47\ P_0$, or $\theta \sim 0.6$ for $S \sim 1$; $\omega = 0$ is called the perveance matched condition and would be the optimum value for beam transmission. In practice, however, the divergence will not go to zero because of optical aberrations in the beam-forming system (finite electrode thickness, distortion of plasma boundary), finite transverse ion energy (emittance), and space-charge forces. One can also use Eq. (11) to relate the variation in divergence to the variation in perveance and hence in plasma density to obtain[32)]

$$\Delta\omega = 16.6 \times S(\Delta n_i/n_i)\ \text{deg.} \tag{12}$$

This predicts that for S = 1, only a 6% variation in plasma density (∿ plasma current) would change the divergence by 1°.

The most common designs of extraction systems use three electrodes (triodes). They consist of a beam-forming electrode (which defines the potential of the boundary of the plasma), an earth electrode, and a suppressor electrode at a small negative potential which prevents electrons from backstreaming to the plasma source (see Fig. 21a).

Other systems in use are four-electrode systems (tetrodes), where a further electrode is inserted between the beam-forming electrode and the suppressor electrode (see Fig. 21b) to control the gradient of the electric field in the extraction gap. It is useful for changing both the beam optics and the electric stress in the electrode structure[34)].

Today extraction systems are mostly designed with the aid of computational methods for the self-consistent electrical fields and particle trajectories. The major contributions of these methods, in addition to their analytical approach, have been the accurate calculation of optimum perveance for special requirement such as maximum current or minimum divergence, and the detailed design of both outlet and extractor electrodes[35)].

REFERENCES

1) H. Winter and B. Wolf, Plasma Physics 16, 791 (1974).
2) J.M. Loiseaux, Nucl. Phys. A354, 415 (1981).
3) G.D. Alton, Proc. Int. Ion Engineering Congress, ISIAT '83 & IPAT '83, Kyoto, 1983, p. 85.
4) H.W. Massay, Negative ions (Cambridge Univ. Press, London, 1976), Ch. 9.
5) R.J. Girnins, C.J. Anderson and L.W. Anderson, Phys. Rev. A16, 2225 (1977).
6) J. Heinemeier and P. Hvelplund, Nucl. Instrum. Methods 148, 65 (1975).
7) J. Heinemeier and P. Hvelplund, Nucl. Instrum. Methods 148, 425 (1975).
8) M. Kaminsky, Atomic and ionic impact phenomena on metal surfaces (Springer Verlag, New York, 1965).
9) V.E. Krohn, J. Appl. Phys. 33, 3523 (1962).
10) J.D. Schneider et al., BNL-51134, 457 (Brookhaven, 1979).
11) R. Keller, Proc. 1984 Linear Accelerator Conf., Report GSI-84-11, Darmstadt (1984), p. 19.
12) R.A. Demirkanov et al., Proc. Int. Conf. on High-Energy Accelerators, Brookhaven, 1962 [BNL 767(C-36), 1962], p. 224.
13) C. Lejeune, Nucl. Instrum. Methods 116, 417 (1974).
14) R. Keller and M. Müller, IEEE Trans. Nucl. Sci. NS-23, 1049 (1976).
15) C. Bieth et al., IEEE Trans. Nucl. Sci. NS-19, 2 (1972).
16) P.M. Mozorov et al., Atomnaya Energiya 3, 272 (1957).
17) A.S. Pasyuk et al., Prib. Tekh. Eksp. 5, 23 (1963).
18) E.D. Donets, IEEE Trans. Nucl. Sci. NS-23, 897 (1976).
19) J. Arianer and R. Geller, Annu. Rev. Nucl. Part. Sci. 31, 19 (1981).
20) J. Faure, Proc. 1984 Linear Accelerator Conf., GSI-84-11, Darmstadt 1984.
21) J. Faure, Proc. Int. Conf. on High-Energy Accelerators, Batavia, 1983 (FNAL, Batavia, Ill., 1983), p. 206.
22) R. Becker, M. Kleinod and H. Klein, 2nd EBIS Workshop, Saclay-Orsay, 1981 (CEA-IN2P3, Orsay, 1981).
23) T. Iwai et al., Phys. Rev. A26, 105 (1982).
24) Y. Yongen and R. Ryckewaert, Proc. Int. Ion Engineering Congress, ISIAT '83 & IPAT '83, Kyoto, 1983, p. 199.
25) K. Prelec and Th. Sluyters, Rev. Sci. Instrum. 44, 1451 (1973).
26) Yu. I. Bel'chenko, G.I. Drinov and V.G. Dudnikov, Bull. Acad. Sci. USSR, Phys. Ser. 39, 91 (1973).
27) K. Prelec, Nucl. Instrum. Methods 144, 413 (1977).
28) K.N. Leimg and K.W. Ehlers, Rev. Sci. Instrum. 53, 803 (1982).
29) J.G. Alessi and Th. Slyuters, Rev. Sci. Instrum. 51, 1630 (1980).
30) W. Gentner and G. Hortig, Z. Phys. 172, 357 (1963).
31) R. Middleton and C.T. Adams, Nucl. Instrum. Methods 118, 329 (1976).
32) J.R. Coupland, R.S. Green, D.P. Hammond and A.C. Riviere, Rev. Sci. Instrum. 44, No. 9 (1973).
33) E. Thompson, Physica 104c, 199 (1981).
34) T.S. Green, Proc. Int. Ion Engineering Congress, ISIAT '83 & IPAT '83, Kyoto, 1983, p. 13.
35) P. Spädtke, GSI Darmstadt Int. Rep., GSI-83-9 (1983).